THz surface wave collapse on coated metal surfaces

Mufei Gong[1], Tae-In Jeon[2] and D. Grischkowsky[1*]

[1]*School of Electrical and Computer Engineering, Oklahoma State University, Stillwater, OK 74078, USA*
[2] *Division of Electrical and Electronics Engineering, Korean Maritime University, Busan 606-791 Korea*
*daniel.grischkowsky@okstate.edu

Abstract: The Zenneck THz surface wave (Z-TSW) on metals is discussed with respect to its difficulty in generation and measurement. The spatial collapse of the extent of the Z-TSW evanescent field, upon the addition of a sub-wavelength dielectric layer on the metal surface, is explained by a simple model, in good agreement with exact analytical theory. Experimental measurements of the THz surface wave on an aluminum surface covered with a 12.5 µm thick dielectric layer have completely characterized the resultant single-mode dielectric layer THz surface wave (DL-TSW). The measured frequency-dependent exponential fall-off of the evanescent wave from the surface agrees well with theory. The DL-TSW frequency-dependent absorption coefficient, phase velocity, group velocity and group velocity dispersion have been obtained. These guided-wave parameters compare favorably with other guided wave structures.

References and links

1. A. Sommerfeld, " Ueber die Fortpflanzung elektrodynamischer Wellen längs eines Drahtes," Annalen der Physik und Chemie **303**(2), 233–290 (1899).
2. J. Zenneck, " Über die Fortpflanzung ebener elektromagnetischer Wellen längs einer ebenen Leiterfläche und ihre Beziehung zur drahtlosen Telegraphie," Annalen der Physik **328**(10), 846–866 (1907).
3. A. Sommerfeld, *Electrodynamics* (Academic, New York, 1952).
4. H. M. Barlow, and A. L. Cullen, "Surface Waves," Proc. IEE **100**, 329–347 (1953).
5. G. N. Zhizhin, M. A. Moskalova, E. V. M. Shomina, and V. A. Yakolev, *"Surface electromagnetic wave propagation on metal surfaces," in* Surface Polaritons Electromagnetic Waves at Surfaces and Interfaces, *V.M. Agranovich and D. L. Mills, eds. (North-Holland, Amsterdam 1982), pp. 93–144.*
6. H. Raether, *Surface Plasmons on Smooth and Rough Surfaces and on Gratings* (Springer, Berlin, 1988).
7. F. Yang, J. R. Sambles, and G. W. Bradberry, "Long-range surface modes supported by thin films," Phys. Rev. B **44**(11), 5855–5872 (1991).
8. T.-I. Jeon, and D. Grischkowsky, "THz Zenneck surface wave (THz surface plasmon) propagation on a metal sheet," Appl. Phys. Lett. **88**(6), 061113 (2006).
9. D. L. Begley, R. W. Alexander, C. A. Ward, R. Miller, and R. J. Bell, "Propagation distances of surface electromagnetic waves in the far infrared," Surf. Sci. **81**(1), 245–251 (1979).
10. E. S. Koteles, and W. H. McNeill, "Far infrared surface plasmon propagation," Intl. J. Infared Mil. Wav. **2**(2), 361–371 (1981).
11. Z. Schlesinger, and A. J. Sievers, "IR surface-plasmon attenuation coefficients for Ge-coated Ag and Au metals," Phys. Rev. B **26**(12), 6444–6454 (1982).
12. K. W. Steijn, R. J. Seymour, and G. I. Stegeman, "Attenuation of far-infrared surface plasmons on overcoated metal," Appl. Phys. Lett. **49**(18), 1151–1153 (1986).
13. D. L. Mills, and A. A. Maradudin, "Surface corrugation and surface-polariton binding in the infrared frequency range," Phys. Rev. B **39**(3), 1569–1574 (1989).
14. J. B. Pendry, L. Martín-Moreno, and F. J. Garcia-Vidal, "Mimicking surface plasmons with structured surfaces," Science **305**(5685), 847–848 (2004).
15. M. Klopfleisch, and U. Schellenberger, "Experimental determination of the attenuation coefficient of surface electromagnetic waves," J. Appl. Phys. **70**(2), 930–934 (1991).
16. J. Saxler, J. Gómez Rivas, C. Janke, H. P. M. Pellemans, P. H. Bolívar, and H. Kurz, "Time-domain measurements of surface plasmon polaritons in the terahertz frequency range," Phys. Rev. B **69**(15), 155427 (2004).
17. J. O'Hara, R. Averitt, and A. Taylor, "Prism coupling to terahertz surface plasmon polaritons," Opt. Express **13**(16), 6117–6126 (2005).

18. L. S. Mukina, M. M. Nazarov, and A. P. Shkurinov, "Propagation of THz plasmon pulse on corrugated and flat metal surfaces," Surf. Sci. **600**(20), 4771–4776 (2006).
19. M. Nazarov, F. Garet, D. Armand, A. Shkurinov, and J.-L. Coutaz, "Surface Plasmon THz waves on gratings," C. R. Phys. **9**(2), 232–247 (2008).
20. J. Zhang, and D. Grischkowsky, "Adiabatic compression of parallel-plate metal waveguides for sensitivity enhancement of waveguide THz time-domain spectroscopy," Appl. Phys. Lett. **86**(6), 061109 (2005).
21. J. D. Kraus, Antennas- Second Edition, (Mc Graw-Hill, New York, 1988).
22. R.E. Collin, *Field-Theory of Guided Waves-* Second Edition (IEEE Press, Piscataway, N.J).
23. H. M. Barlow, and J. Brown, *Radio surface waves* (Oxford, Clarendon Press, 1962).
24. J. C. G. Lesurf, "Beam coupling, lenses and mirrors," in *Millimetre-wave Optics, Devices and Systems* (Adam Hilger, Bristol and New York, 1990), pp. 11–28.
25. G. I. Stegeman, and R. J. Seymour, "Surface plasmon attenuation by thin film overlayers in the far infrared," Solid State Commun. **44**(9), 1357–1358 (1982).
26. S. S. Attwood, "Surface-Wave Propagation over a coated plane conductor," J. Appl. Phys. **22**(4), 504–509 (1951).
27. Y. Zhao, and D. Grischkowsky, "Terahertz demonstrations of effectively two-dimensional photonic bandgap structures," Opt. Lett. **31**(10), 1534–1536 (2006).
28. C. A. Balanis, *Advanced Engineering Electromagnetics* (Wiley, 1989).
29. A. W. Snyder, and J. D. Love, *Optical Waveguide Theory* (Kluwer Academic Publishers, 2000).
30. R. Mendis, and D. Grischkowsky, "Plastic ribbon THz waveguides," Appl. Phys. Lett. **88**, 4449–4451 (2000).
31. M. Gong, *Study of THz Surface Waves (TSW) on Bare and Coated Metal Surfaces* (Ph. D dissertation of Oklahoma State University, Stillwater, 2009).
32. T.-I. Jeon, J. Zhang, and D. Grischkowsky, "THz Sommerfeld wave propagation on a single metal wire," Appl. Phys. Lett. **86**(16), 161904 (2005).
33. R. Mendis, and D. Grischkowsky, "Undistorted guided-wave propagation of subpicosecond terahertz pulses," Opt. Lett. **26**(11), 846–848 (2001).
34. G. P. Agrawal, Fiber-Optic Communication Systems, 3rd ed. Series in Microwave and Optical Engineering *(New York, John Wiley & Sons Inc. 2002).*

1. Introduction

The experimental observation at microwave and THz frequencies of the single mode electromagnetic (EM) surface wave on a metal sheet has proven to be extremely difficult due to the large extent of the wave from the surface and to the very weak guiding by the surface. The theoretical study of this wave started with Sommerfeld's study of EM propagation on a single metal wire [1], followed by Zenneck's theoretical description of EM propagation on a flat metal surface [2]. Both studies were done more than a century ago. The Zenneck EM surface wave single mode solution only exists for finite conductivity; for a perfect electrical conductor, the Zenneck surface wave vanishes [3]. Barlow and Cullen have written an excellent overview [4] of the early surface wave investigations. A good description of surface wave measurements and experimental techniques is presented in the more recent work [5]. Raether has given a good description of the Zenneck surface wave from the equivalent point of view of surface plasmons [6], and a complete mathematic summary has been presented [7].

A recent experimental study [8] of the propagation of THz pulses as THz surface waves (TSWs) on a metal sheet measured a much higher attenuation than predicted by theory [1–7]. In earlier work such pronounced disagreement between theory and experiment has resulted in a long standing and unresolved controversy [8–19]. At microwave and THz frequencies (far-infrared) it has always been experimentally difficult to distinguish between the freely propagating EM radiation along the metal surface and the guided surface wave [8–19], due to their collinear propagation and essentially equal phase velocities. To obtain the predicted large propagation distances extremely flat and optically smooth surfaces appear to be required [10,13]. Surface roughness has been predicted to bind the wave more tightly to the surface and to thereby increase the attenuation [13]. It has also been shown that a small amplitude grating on the surface can tightly bind the surface wave, even for a perfect conductor [13], and that more generally for a perfect conductor; it is possible to spoof surface plasmons with subwavelength structured surfaces [14]. Subwavelength layers of high-index, low-loss dielectrics on the metal surface can reduce the extent of the evanescent field by an order of magnitude, thereby causing much higher propagation loss [11–13]. In addition, the sensitivity to the dielectric layer has been discussed for sensor applications [16].

In this report we first discuss the fundamental problems associated with the efficient generation of the Zenneck THz surface wave (Z-TSW) on a metal sheet, using a transverse

electromagnetic (TEM) mode parallel plate waveguide (PPWG) [8]. Here, the output end of the waveguide is adiabatically opened to a 1.2 mm final separation [20], where one surface
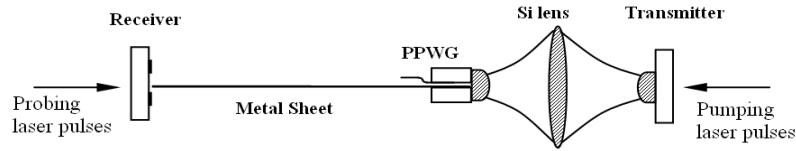

Fig. 1. Cross-section detail of the surface wave setup.

is the coupling metal sheet for the Z-TSW. This approach (described in detail in the experimental section) is illustrated above in Fig. 1, where fs laser pumping pulses drive the THz transmitter. The resulting subps THz pulses are efficiently focused by the three silicon lenses into the PPWG. The THz pulses from the output face of the PPWG with the 1.2 mm slit opening are coupled onto the metal sheet. At the output end of the metal sheet, the transmitted THz pulses are measured by the THz receiver, driven by fs laser probing pulses.

As will be discussed in the theory section, the experimental requirements to generate the Z-TSW are extremely demanding, requiring matching the plane-wave field profile of the Z-TSW with a plane-wave excitation beam. The fact that these requirements have not yet beemet in the previous experimental work, explains the absence of definitive and measurable Z-TSW propagation. However, there are leaky THz surface waves that are not truly stable transverse solutions of wave equation [21,22]. These leaky TSWs can propagate distances of many cm and can be excited and detected. These waves will also appear in the numerical simulations depending upon the method of excitation. Consequently, because the experimental spatial scale was not consistent with the extensive sizes required by the spatially large Z-TSW, many experimental observations of THz surface waves appear to be dealing with the leaky waves and not the Z-TSW. This applies to the results of the Ref. 8, which clearly described measurements of a type of THz surface waves.

We have observed that the addition of a thin dielectric layer with a thickness only of the order of the wavelength/50 on the metal surface causes the evanescent field to spatially collapse by approximately 200 times (compared to that of the uncoated metal). We have explained this powerful effect by an accurate and simple model, which agrees with our definitive experimental characterization of the DL-TSW for the coated surface. For this case our experimental arrangement similar to Fig. 1 achieves almost complete coupling from the PPWG into the DL-TSW. In addition, the DL-TSW guided-wave parameters compare favorably with those of other guided-wave structures.

2. Theoretical approach

2.1 Discussion of the bare metal surface

On the bare metal surface, the Z-TSW transverse field distribution is the Zenneck single mode surface wave solution determined by the metal conductivity [1–7]. In the THz range, the real part of the metal conductivity is quite high and can be considered to be a frequency-independent constant equal to the handbook dc value of $\sigma_0 = 3.54 \times 10^5/(\Omega \text{ cm})$ for Al. It is important to note that both the Zenneck surface wave theory [2–5] and surface plasmon theory [6,7], are equivalent for Z-TSW pulse propagation with the propagation constant $k = k_r + ik_i$ on a metal sheet. At 0.5 THz we obtain the complex dielectric constant for Al as $\varepsilon = \varepsilon_r + \varepsilon_i = -3.3 \times 10^4 + i\, 1.28 \times 10^6$ [27]. For the THz high conductivity case the Z-TSW phase velocity is only slightly less than c by 1 part in 10^8, consequently we set $k_r = k_0$. A phase velocity less than c is consistent with the general k vector dispersion curve for surface waves, where the k vector is always below the light line as shown by Fig. 2(b) in [6]. The relationship for $k_i = \alpha$ simplifies to $\alpha = k_0/(2\varepsilon_i)$, for $k_0 = 2\pi/\lambda_0$ with λ_0 designating the free-space wavelength. Calculating α for our parameters we obtain the extremely small value $\alpha = 0.0041$ m^{-1}, corresponding to the very large, metal-surface, guided wave propagation length of L = 244 m, where $k_i L = 1$ gives the distance at which the Z-TSW amplitude decays to 1/e of its initial

value. In the air above the metal sheet, theory predicts that the field amplitude falls off exponentially from the surface as $\exp[-\beta(\omega) y]$ for the y axis perpendicular to the surface. For our high-conductivity case, $\beta = [2k_r k_i \exp(i\pi/2)]^{1/2}$, which simplifies to $\beta = [k_0 (2 \varepsilon_i)^{-1/2}] [1 + i] = \beta_0 (1 + i)$. In Fig. 2, we present the normalized intensity (power) fall-off from the metal surface with the function $\exp [-2 \beta_0 y]$, together with actual field fall-off described by $(\exp [-\beta_0 y]) (\cos \beta_0 y - i \sin \beta_0 y)$. This expression describes an exponential field decay with increasing distance from the metal surface, together with progressive phase increase for a wave traveling towards the surface. Consequently, there is a power flow to the surface due to the ohmic losses of the propagating Z-TWS. See Eqs. (4) and 5 in Barlow and Cullen [4]. We show $\exp [-\beta_0 y] (\cos \beta_0 y)$ in Fig. 2(b) which falls off significantly faster than $\exp [-\beta_0 y]$. Evaluating β_0, we obtain $\beta_0 = 0.065$ cm^{-1} for 0.5 THz giving an evanescent field extending 15.3 cm above the surface to fall off by $1/e$, showing that the Z-TWS is very weakly coupled to the bare metal surface.

In contrast, for the considered experimental configuration of Fig. 1, the freely propagating wave from the 1.2 mm launching PPWG aperture keeps expanding due to diffraction, which adds complexity to the Z-TSW launching process and is associated with the long standing controversy between theory and experiment [8–19]. Consequently, it is informative to assess the diffraction from the output waveguide in more detail. The diffraction from the 1.2 mm wide slit opening of the waveguide is equivalent to single slit diffraction with a conducting sheet extending in the propagation direction from one edge of the slit. Because of the Al sheet's mirror effect, the equivalent diffraction slit width should be doubled to 2.4 mm, where the Al sheet is the centered symmetric plane. The far-field, amplitude diffraction pattern of the single slit is described by the $(\sin\theta)/\theta$ function with the central maxima at the metal surface.

Figures 2(a) and (b) show the overlapped intensity and field profiles of the Z-TSW and the diffracted wave at a few selected propagation distances for $\lambda = 600$ μm (0.5 THz) on an aluminum surface. During the propagation, the Z-TSW field pattern is constant and is shown as the line with shaded area (yellow in the on line version), with $1/e$ amplitude value of 15.3 cm. The evolving diffraction patterns at propagation distances D of 20 cm, 91 cm, 180 cm, 5 m and 50 m from the slit are also plotted. The Z-TSW fields and diffracted wave field are normalized to unity at 20 cm for comparison. At the propagation distance of 122 m for 0.5 THz, the intensity of the Z-TSW drops by $1/e$ due to absorption by the metal, while the $1/e$ extent of the diffracted wave amplitude is 28 m, compared to the unchanging extent of the Z-TSW with a $1/e$ amplitude extent of 15.3 cm. An important point is that the two waves propagate with the same phase velocity to 1 part in 10^8.

The surface wave launching/coupling efficiency is determined by the overlap integral of the excitation field (the TEM mode of the PPWG) and the Z-TSW field [23,24]. The overlap integral is the scalar product of the two fields integrated over a plane. If the two beams are plane waves, the overlap integral simplifies to the integral of the product of the two field patterns, which it does in this case. Calculating power coupling into the Z-TSW wave via the
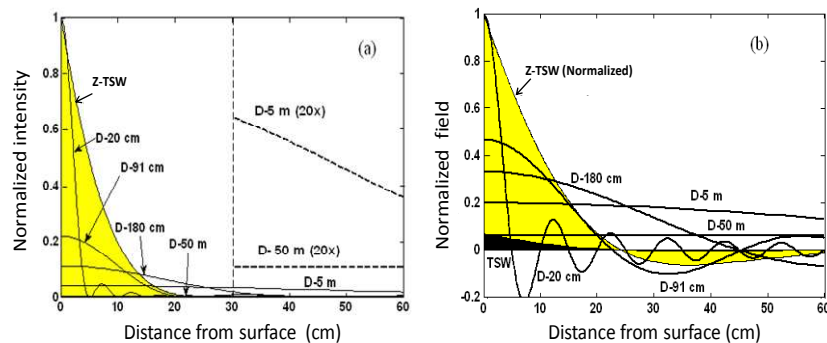

Fig. 2. (a) Intensity curve of surface wave and diffracted wave field for $\lambda_0 = 600$ μm. (b) Field overlap of the bare metal surface wave field (curve of yellow area) and diffracted field.

overlap integral gives the very small value of 1.5% at 0.5 THz, mainly due to mis-match of the output slit width of 1.2 mm and the more than 15 cm extent of the Z-TSW. In the perfect conductor case all of the power would go into the diffracted wave. Here, we have 1.5% of the total power going to the Z-TSW and 98.5% going to the diffracted wave. Given these relative figures, the predicted relative amplitude comparison of the 0.5 THz component of the Z-TSW drops to the solid black curve starting at 0.068 at the metal surface. It is important to note that the Z-TSW field is less than the diffracted field, even out to the propagation distance of 50 m. Also, due to the Z-TSW being a plane-wave and the diffracted wave being a cylindrical wave with radius equal to the propagation distance, the two waves will interfere with each other in the measurement plane normal to the metal sheet. At the metal sheet they are in phase.

In order to dramatically increase coupling to the Z-TSW, the experimental setup would need to be scaled up in size to the 1/e extent (15 cm) of the Z-TSW. This would require, referring to Fig. 1, a PPWG of at least 15 cm wide focused by a cylindrical lens more than 15 cm long to focus an incoming THz beam with a beam waist diameter of more than 15 cm at the cylindrical lens. The adiabatically opening PPWG would need to be 1 m long to include an adiabatically opening S curve (in cross section) opening to 15 cm at the output face, and maintain linear polarization and a plane-wave phase front for optimal coupling. These very large dimensions and requirements are clearly unworkable. An alternative more workable arrangement would be that shown in Fig. 3 to produce a plane wave with a beam waist of 20 cm at a metal slit aperture of 15 cm. This design is still a compromise, because the lateral extent (x axis length) should be several times larger than the fall-off distance, of 15 cm, which would require a 1 m long THz line source and a 1 m long 2D parabolic mirror.
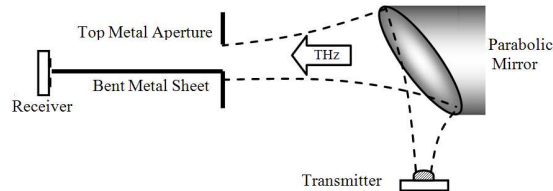

Fig. 3. A proposed large-scale TSW coupling arrangement.

2.2 Dielectric coated surface

As an experimental solution to the weak coupling of the Z-TSW to the bare metal surface, a thin dielectric coating greatly compresses the TSW spatial extension and thereby greatly improves the surface wave coupling [4,25]. The dielectric coating confines the TSW field to within only a few wavelengths from the surface. Figure 4 shows the comparison of the calculated TSW transverse fields on a bare and a coated metal surface, illustrating the field collapse due to the film.

As shown in Fig. 4(a), on a bare metal surface, the Z-TSW field extends to hundreds of wavelengths due to the high metal conductivity. Due to the binding effect of the thin (~$\lambda/50$) 12.5 µm dielectric film shown in Fig. 4(b), the DL-TSW field extension is greatly compressed (approximately 180 times) to a few wavelengths from the surface. It is interesting to note that the 1/e field extension for the DL-TSW at 0.5 THz for a 5 µm thick dielectric layer increases to 3.4 mm, and for a 25 µm layer, it decreases to 0.65 mm. This dynamic response is clearly of importance for sensing applications [16].

The dielectric coated metal surface structure is shown in the Fig. 5(a). General modal analysis of this structure is complicated, because of the complex metal conductivity [11,25,26]. However, in the THz range the problem can be viewed in a much simpler way; because, the real part of the metal conductivity is quite high and can be considered to be a frequency independent constant equal to the handbook dc value (for aluminum, $\sigma_r = 3.54 \times 10^5/(\Omega \text{ cm})$), in contrast to the frequency-dependent metallic conductivity at optical frequencies (for $\lambda = 800$ nm, $\sigma_r = 1.2 \times 10^3/(\Omega \text{ cm})$ [27].
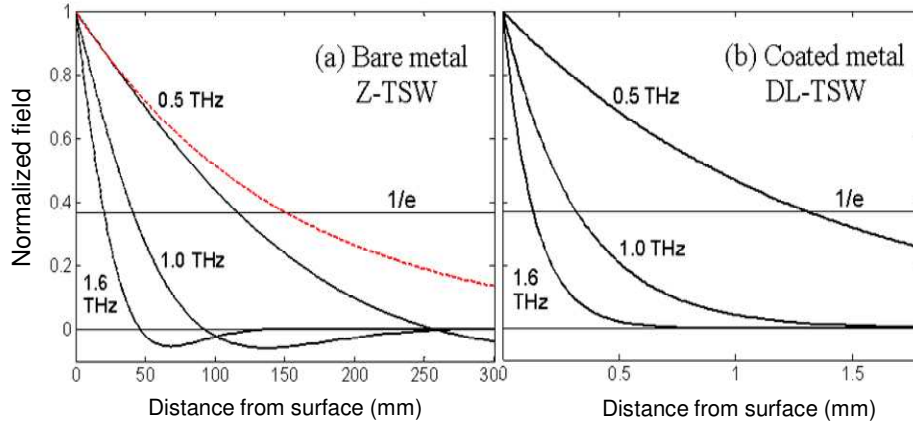
Fig. 4. Calculated collapse of the evanescent field due to the dielectric film. (a) Bare aluminum surface. (b) Aluminum surface coated with 12.5 μm polyethylene film (n = 1.5). Solid lines show exp [-β₀y] (cos β₀y) dependence. Dashed line (red on-line) shows exp [-β₀y] dependence for 0.5 THz, giving the 153 mm fall-off distance.
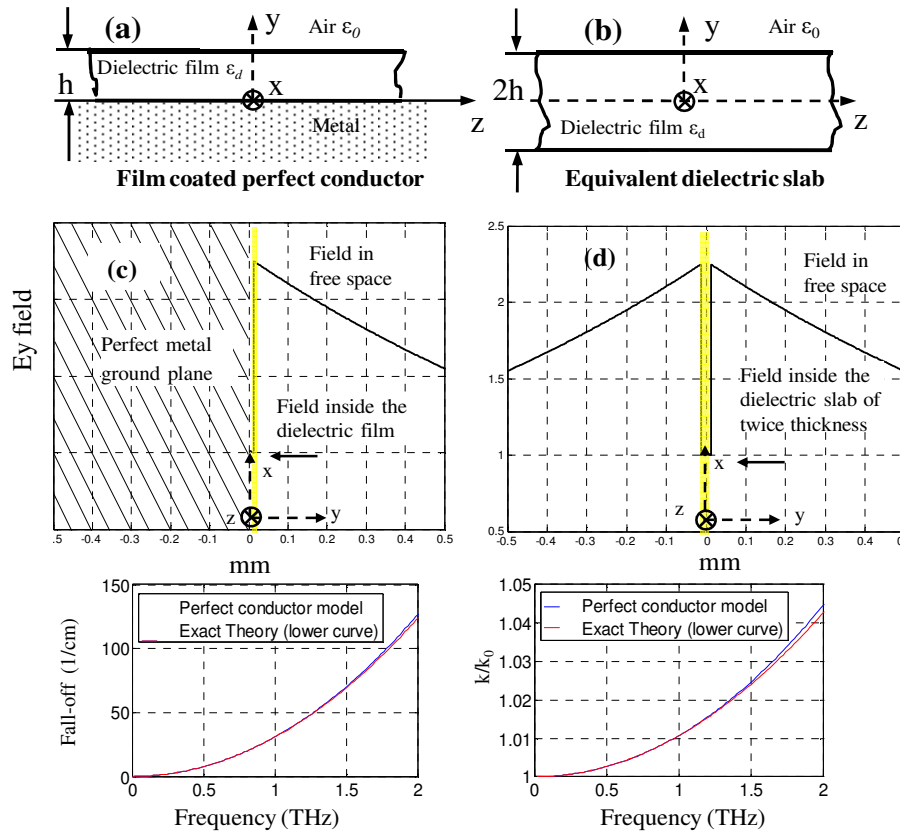

Fig. 5. Theoretical equivalence of slab waveguide structure, if the conductivity in (a) is infinite, then its field distribution is equivalent to the upper half of (b); (c) E_y field profile of coated surface. (n = 1.5) film thickness 12.5 µm; (d) E_y field of the dielectric slab waveguide, TM_0 mode at 0.5 THz; Simple model vs. exact theory (e): Exponential fall-off constant; (f) ratio of propagation constant $k = 2\pi\, n_e\, /\lambda_0$ to free space wave vector $k_0 = 2\pi\, /\lambda_0$.

Therefore, for THz frequencies the coated metal surface in Fig. 5(a) can be viewed (to a very good approximation) as the classic dielectric slab waveguide on a perfect conductor, also

called the grounded dielectric film waveguide [28]. The perfect conductor plane is treated as a symmetric plane, and the problem is equivalent to solving a waveguide that is composed of the film and its mirror image, which in turn is equivalent to a free-standing dielectric slab waveguide with twice the thickness as shown in Fig. 5(b). Therefore, the problem of the surface wave is simplified to the textbook analysis of the dielectric slab waveguide [28–31].

For a very thin ($\sim\lambda/20$) dielectric slab waveguide, only the dominant TM_0 mode propagates, and the surface waveguide structure is working in the single TM_0 mode with features similar to the Z-TSW, but existing as a perfect conductor solution. Figure 5(d) shows the TM_0 mode E_y field solution of a 25 μm dielectric slab (n = 1.5) waveguide at 0.5 THz. Inside the film, the E_y field changes as cos [β_d y] with β_d = 117/cm. At the dielectric-air boundary (y = h), the E_y field increases by the multiplicative factor $\varepsilon_d/\varepsilon_0$. Outside the film, the E_y field decreases with y as the exponential function exp[-β_o (y-h)], where at 0.5 THz the fall-off constant β_o = 7.64 cm^{-1}. For the coated metal surface structure with a 12.5 μm dielectric film, the field profile in Fig. 5(c) is the right half of Fig. 5(d).

Treating metal as a perfect conductor at THz frequencies has greatly simplified the problem. Earlier researchers solved the general wave equation of the surface wave on coated metal using the actual frequency dependent metal dielectric constant, which must be used for the optical range [7]. The general solutions for exponential fall-off constants on coated metal are compared to the simple solutions in Figs. 5(e) and (f). Not surprisingly, the two curves almost overlap which demonstrates that the perfect-conductor treatment is an accurate assumption for THz frequencies, similar to the usual approach in microwave theory, which assumes perfect conductivity to derive the modes of metal waveguides.

3. Experimental Apparatus

The schematic of the experimental setup is shown as Fig. 6 below [30]. A beam of 800 nm, 60 fs laser pulses from a Ti:Sapphire laser operating at 83 MHz is split into two beams: one goes to the transmitter as the pumping pulses and the other goes to the receiver as the probing pulses. For the transmitter, when the laser pulses are focused onto the transmitter chip, THz pulses are generated with the E field vertically polarized. The generated ps THz pulses pass through the three silicon lenses L_1, L_2 and L_3 and are focused into the entrance slit of the metal PPWG. The plano-cylindrical lens L_3 produces a line focus on the input air gap of 100 μm between the two Al plates of the PPWG, thereby coupling the THz pulses into the waveguide. The PPWG is the starting part of the surface wave apparatus, which is shown in the dashed box 1.
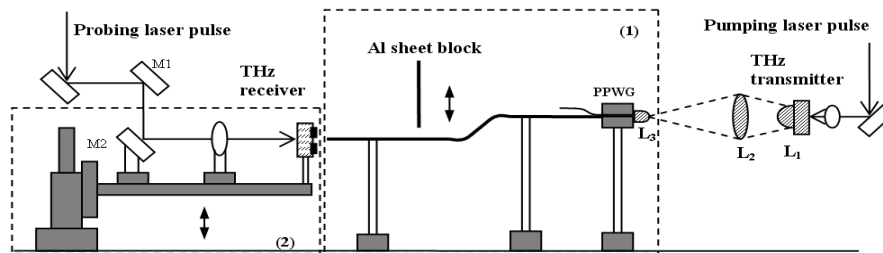

Fig. 6. 2D schematic of the system setup.

Figure 7 shows the detailed structure of the surface wave apparatus. The TSW propagates on a 24-cm-long by 10-cm-wide by 100-μm-thick sample Al sheet, for which the surface is tightly covered with 12.5 μm polyethylene film with refractive index n = 1.5. An extension of the covered Al sample sheet is placed into the PPWG on top of the lower plate of the waveguide to couple the THz wave onto the Al sheet. On top of the sample Al sheet, there is another 3.5 cm long Al sheet with 100 μm separation from the bottom sheet to form the actual parallel plate structure. The TSW is launched at the extended PPWG waveguide aperture; the two waveguide sheets make an adiabatically opening structure with an output slit width of 1.2 mm to realize the excitation of the surface wave.
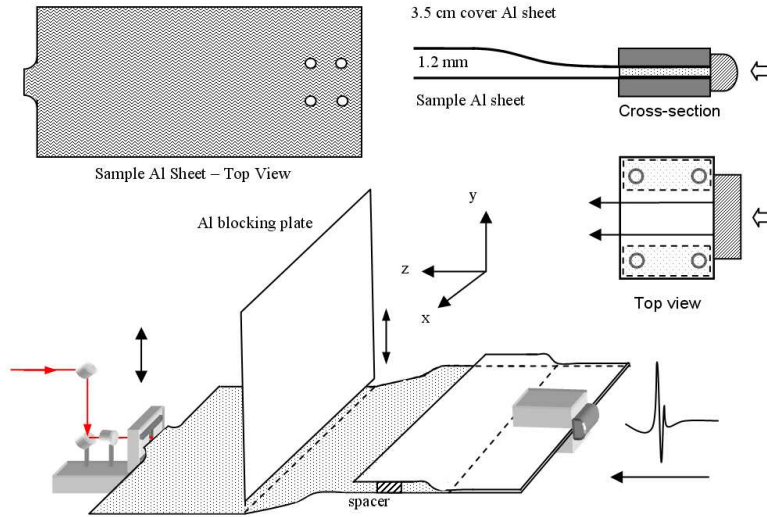
Fig. 7. Assembling drawing of surface wave sample.

During the launching process, along with the surface wave, there is always a freely propagating THz diffraction wave coming from the 1.2 mm output slit aperture. To distinguish this part of the wave in the received signal, a 3.5 mm-deep adiabatic curve is made as shown in Figs. 6-8. Then a 10 cm wide Al blocking plate is vertically placed after the curve with a 3 mm opening between the bottom edge of the plate and the sheet surface. The blocking plate is positioned 8 cm from the end tip of the Al sheet, and correspondingly 12 cm from the 1.2 mm opening of the extended PPWG.
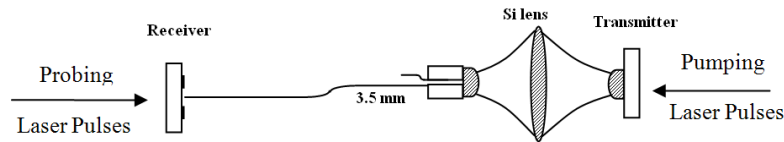
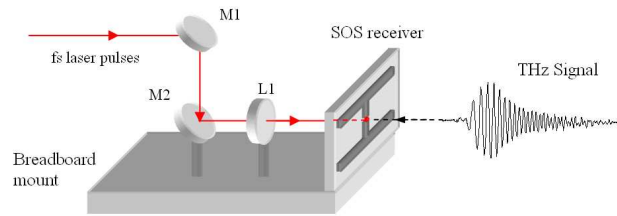Fig. 8. Detail of the THz surface wave setup.

Fig. 9. 3D view of THz receiver of the dashed box 2.

The receiver (dashed box 2, Fig. 6) is located at the end of the sheet to detect the TSW field that is polarized perpendicular to the sheet surface, as shown in Figs. 6-8. The receiver chip is lithographically fabricated on a double-side polished silicon-on-sapphire (SOS) wafer, so that the laser sampling beam can pass through the sapphire substrate and then irradiate the silicon layer in the gap between the two arms of the antenna. The metal antenna is closely placed near the edge of the sheet (distance less than 30 μm) for direct detection of the THz electrical field. As shown in Figs. 6 and 9, a periscope mounting configuration is used to enable the vertical movement of the receiver. The receiver and two optics (M2 and the optical lens L1) are mounted together on a breadboard so that they can move vertically to measure the DL-TSW field at different heights relative to the surface.

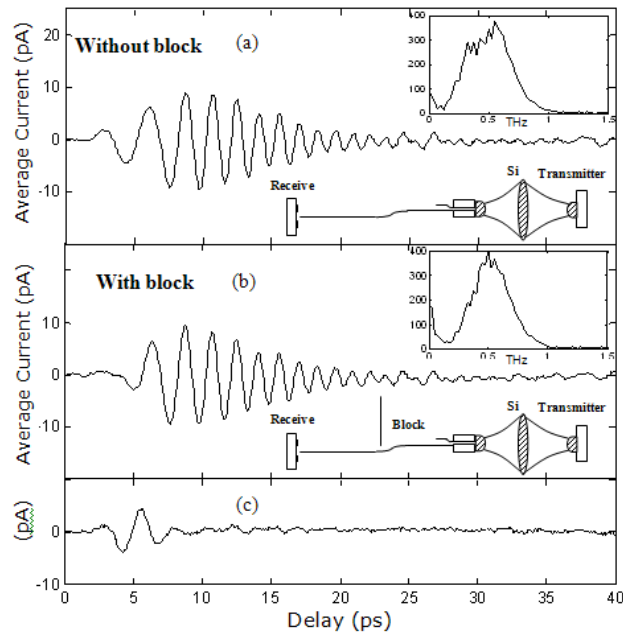# 4. Experimental results and discussion

Fig. 10. (a) TSW pulse on coated surface without block. (b) TSW pulse on coated surface with block (c) The freely propagating diffraction wave given by subtraction of TSW pulse (b) from TSW pulse (a). Inserts show corresponding spectra.

On the dielectric coated metal surface, the DL-TSW field has stronger coupling and surface confinement; therefore, diffraction is no longer the dominant effect in the received signals, compared to the case of bare metal surface. This is shown by the comparison made in Fig. 10, the top curve (a) is the signal taken without the blocking plate, and the middle curve (b) is taken with the 3-mm gap blocking plate. This observation indicates that with the improved coupling due to the dielectric film, almost all of the energy is being carried by the surface wave mode propagating closely along the surface. The blocking plate has very limited influence. The unguided freely propagating diffraction wave is obtained by subtraction of curve (b) from curve (a) giving curve (c). As shown in Fig. 10(c), the freely propagating diffraction wave is the small leading part of the signal which propagated along the shorter straight line path.

For this case, the power coupling given by the overlap integral between the PPWG TEM mode (modified by the dielectric layer) and the DL-TSW field is quite good. At 0.5 THz the power transfer is 60%.

Signals at different heights above the surface are measured by vertically moving the receiver. The time delay effect due to this height change of the receiver has to be compensated to obtain the actual arrival time of each signal. For example, in the Fig. 11(a), the lower curve was taken at the surface and the upper curve was taken 0.60 mm above the surface, where it can be seen that there is an apparent time delay between the two signals. As shown in Figs. 6 and 9, when the receiver is moved upward by 0.60 mm, the distance between M1 and M2 becomes shorter by 0.60 mm, and therefore the optical sampling pulse will arrive at the receiver 0.60 mm/c = 2.00 ps earlier. However, the arrival timing of the THz pulse signal remains the same. Therefore, in order to compensate for this time delay, the signal above the surface needs to be moved to 2.00 ps earlier in time relative to the signal on the surface. Figure 11(b) shows that after removing the effect of vertical position change of the receiver, the peaks in the surface wave pulse at 0.6 mm above the surface are aligned precisely with the corresponding ones in the pulse on the surface except for their smaller amplitudes.
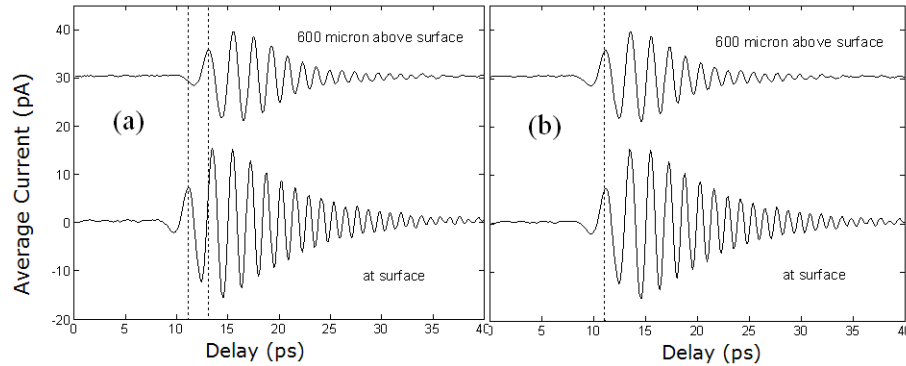
Fig. 11. THz surface wave pulses measured at the surface and at 0.60 mm above surface. (a): Before compensating the time delay caused by receiver movement. (b): After compensation.
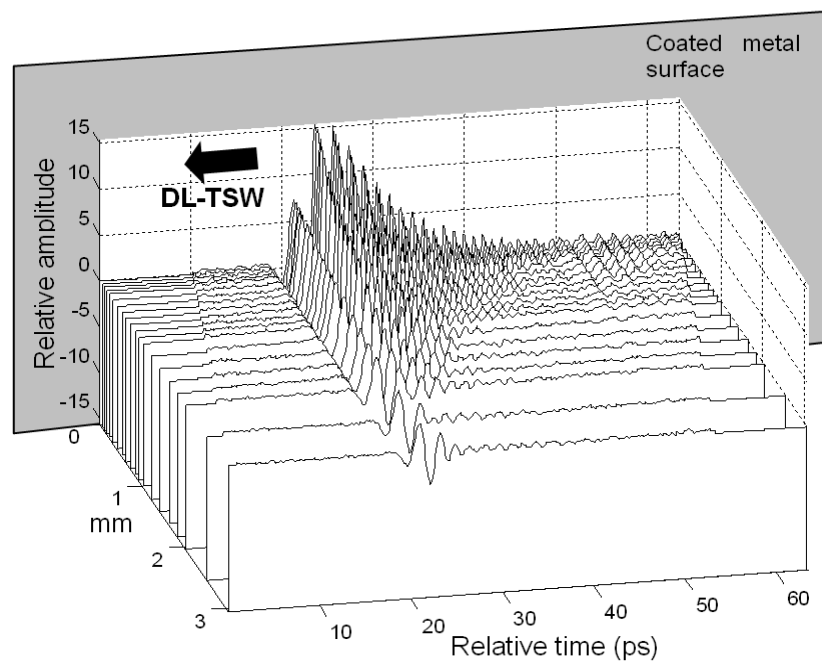

Fig. 12. Time domain DL-TSW waveforms measured at different distances from surface.

As the receiver moves up from the surface, a DL-TSW field fall-off is observed. In Fig. 12, the time domain signals are plotted according to their corresponding vertical positions. It clearly shows a snapshot of the entire incoming THz surface wave, and gives the field fall-off profile above the surface. Because all the time shifts have been compensated, the displayed relative positions of the waveforms in time reflect their actual arrival timing. This again shows that the DL-TSW at different heights above the surface hits the receiver at the same time, as expected according to the plane-wave mode profile; the entire wavefront propagates with the same velocity. It is also worth noticing that the long ringing tail of high frequency components fade away more rapidly, as the wave extends higher into space
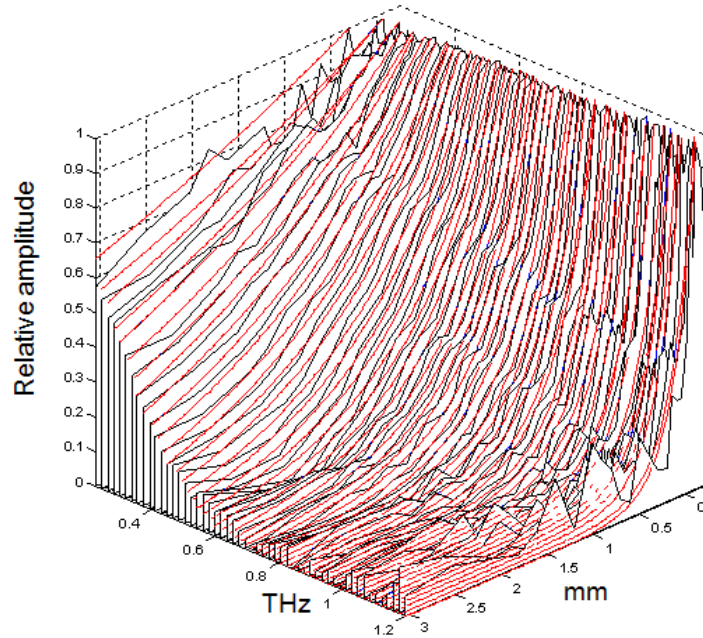
Fig. 13. Overlapped view of the frequency dependent field fall-off measurement (black) of the coated metal surface with the corresponding theoretical field fall-off (red). Distance from the surface is given in mm and frequency in THz.

The frequency dependence of the evanescent field fall-off of the surface wave is better presented in the frequency-domain. Fourier transforms were performed on the time domain signals of Fig. 12, to obtain the corresponding amplitude spectra at the different receiver positions. By putting the spectra together in the order of their corresponding receiver positions, the amplitude fall-off of the surface wave can be compared in frequency-domain.
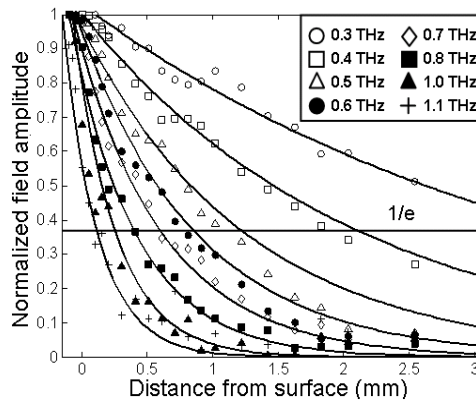

Fig. 14. Experimental and theoretical field fall-off at selected frequencies.

Then for each frequency, a spatial amplitude fall-off distribution was obtained. Figure 13 shows the spectra vs distance from the dielectric coated metal surface to 3 mm above the surface.

Because the amplitude is maximum at the surface, all the amplitudes are normalized to the amplitude at the surface for a clearer comparison of the amplitude fall-off curves from 0.2 to 1.2 THz. The theoretically calculated DL-TSW field fall-off pattern (plotted in red) shows good agreement with experiment.

The comparison between experiment and theoretical exponential field fall-off of dielectric-coated surface can also be observed in Fig. 14. The theoretical field fall-off $\exp[-\beta_0 (y-h)]$ and

experimental field fall-off curves at selected frequencies are compared with reasonably good agreement. Note that in Figs. 13 and 14 not all frequencies show their peaks at the surface level (y = 0). This is believed to be due to the small separation (30 microns) between the end of the surface sheet and the receiver chip. The surface wave diffracts at the edge of the surface causing the slight shift of the y position of the maximum amplitude. In the ideal case for which the detector would be located at or above the surface, rather than at the edge, all the peaks should show up at the y = 0 surface level.

To further test our understanding, a numerical simulation was performed to calculate the output DL-TSW. Three processes are considered to be responsible for the reshaping of the DL-TSW signal: 1. The dispersion relation, which accounts for the frequency dependent phase delay. This process introduces chirping into the DL-TSW pulse and explains the long lasting ringing. 2. The absorption, this relatively small effect introduces some frequency dependent amplitude attenuation to the output signal. 3. The coupling between different elements of the system, e.g. the Fresnel amplitude transmission coefficient of the silicon cylindrical lens is 70%. Other uncalculated frequency-independent coefficients have only slight effects on the pulse magnitude and shape.
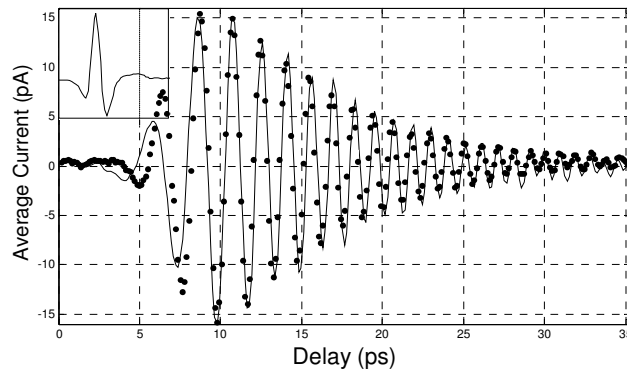

Fig. 15. Comparison of the experimental (dots) and theoretical (solid line) time domain curves. The insert shows the input pulse with a peak to peak amplitude of 65 pA.
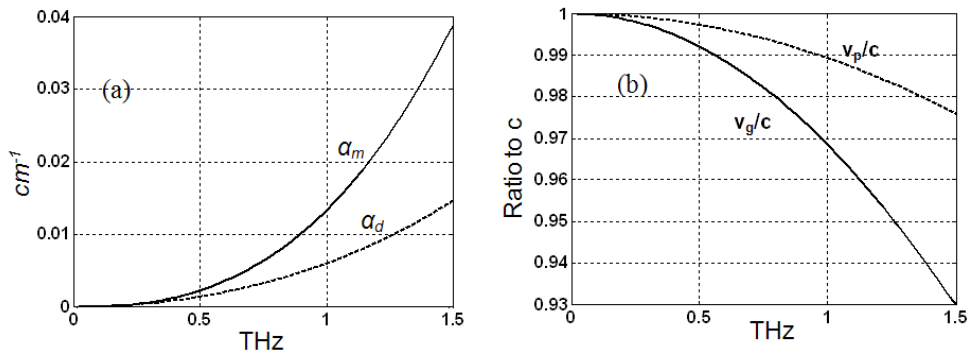

Fig. 16. (a) The amplitude absorption coefficient due to the dielectric (lower line) and metal (upper line); (b) Ratio of phase velocity v_p over c (upper line) and ratio of group velocity v_g over c (lower line).

Therefore, given the free space input signal spectrum, the output signal spectrum was theoretically evaluated. An inverse Fourier transform was performed on the calculated spectrum, to obtain the theoretical time domain signal in Fig. 15, showing excellent agreement with experiment, and demonstrating that the surface wave on dielectric coated surface is well understood and well reproduced by experiment.

Compared to other guided-wave structures, the characteristics of the DL-TSW on the dielectric-coated metal surface are quite good. For example, below 0.5 THz the absorption is

less than that of the single-wire Sommerfeld wave and the comparable coax [32]. The absorption coefficient $\alpha(\omega)$ is the sum of that due to the dielectric $\alpha_d(\omega)$ and that due to the metal $\alpha_m(\omega)$. For our 12.5 µm case, assuming the power absorption coefficient of bulk polyethylene to be 0.5 cm^{-1} below 1.5 THz and using the handbook value for the electrical conductivity of aluminum, we obtain the amplitude absorption coefficients α_d and α_m as shown in Fig. 16(a) [28–31]. The DL-TSW structure has significant dispersion compared to the essentially dispersion free propagation in the metal PPWG [33].

The calculated phase and group velocities over our frequency band are presented in Fig. 16(b). At first sight, these curves look significantly different than those obtained earlier for 120 µm and 150 µm thick plastic ribbon THz waveguides [30]. However, these curves are quite similar to a truncated version of those of Ref. 30, for frequencies less than the ratio of slab thickness/wavelength equal to 25µm/200µm = 1/8. This limit guarantees the slab is much thinner than the free space wavelength, which is the case for Fig. 16(b). For a thinner 5 µm film, α_d and α_m are reduced to approximately 1/7 and 1/3 of that of the 12.5 µm film, respectively. Similar strong reductions are obtained for the dispersion of the phase and group velocity.

For the 12.5 µm film, the group velocity dispersion (GVD) is well approximated by the simple relationship GVD = 0.35 f in units of (ps)^2/cm and where the frequency f is in THz, e.g. for f = 1.5 THz, GVD = 0.53 (ps)^2/cm. In order to understand the GVD parameter, first note that the propagation constant k in Fig. 5 (f) is $k = \omega/v_p$ and that $k_1 = dk/d\omega = 1/v_g$ and that GVD is defined as $k_2 = d^2k/d\omega^2$ [34]. The usefulness of this definition is seen by the following explanation. The time required for a pulse to propagate through a waveguide of length L is $t = L/v_g$. This relationship is the same as $t = Lk_1$. From this result it is obvious that the difference in transit times Δt for pulses of different frequencies is given by $\Delta t = Lk_2\Delta\omega$, where $\Delta\omega$ is the angular frequency difference between the pulses [34].

5. Summary and Conclusions

The theoretical discussion of the Zenneck THz surface wave described the very large spatial extent of the evanescent field of the Z-TSW associated with the very weak guiding of this wave by a smooth metal surface. The Z-TSW is the principle mode for electromagnetic metal surface propagation and has remarkably low loss and low group velocity dispersion; the Z-TSW does not exist for a perfect conductor. In addition, there are leaky THz surface waves that are not truly stable transverse solutions of the wave equation [21,22]. These leaky TSWs can propagate distances of many cm and can be excited and detected. These waves will also appear in numerical simulations depending upon the method of excitation. Consequently, many experimental observations of THz surface waves appear to have been dealing with these leaky waves and not the Z-TSW, because the experimental spatial scales were not consistent with the extensive sizes required by the Z-TSW.

In contrast, the dielectric layer THz surface wave can be quantitatively explained by a simple model which assumes that the dielectric layer is on a smooth surface of a perfect conductor. This simple model is equivalent to a free-standing dielectric waveguide of twice the thickness of the dielectric layer. For thicknesses much smaller than the wavelength, the propagation solution is the fundamental TM_0 mode of the dielectric waveguide, which has an exponential fall-off of the fringing field (evanescent field) similar to the Z-TSW, but with a 100-fold reduced spatial extent . The DL-TSW is strongly bound to the surface and is an analytic solution to the wave-equation for a perfect conductor.

The 100-fold reduction (compared to the Z-TSW) in the spatial extent of the evanescent field of the DL-TSW with a thin 12.5 µm dielectric surface layer has enabled the complete experimental characterization of the DL-TSW. Highly efficient coupling into the surface layer DL-TSW was achieved using a metal parallel plate waveguide as the coupler to an input freely propagating THz pulse. The guided wave parameters for the DL-TSW compare favorably with other waveguide structures. Unlike the grating or surface corrugation technique, effective for only a single frequency, the thin film coating enhances the DL-TSW field confinement of all the frequencies in a relatively large range, and clearly has potential for sensing applications.

Acknowledgments